Mem. S.A.It. Vol. 76, 372

Memorie della

Launching jets from resistive accretion disks

C. Zanni[1], A. Ferrari[1], S. Massaglia[1], G. Bodo[2] and P. Rossi[2]

[1] Dipartimento di Fisica Generale dell'Università, Via Pietro Giuria 1, I - 10125 Torino email: zanni@ph.unito.it

[2] INAF – Osservatorio Astronomico di Torino, Strada dell'Osservatorio 20, I-10025 Pino Torinese email: bodo@to.astro.it

Abstract. We present numerical time-dependent MHD simulations of the acceleration and collimation process of astrophysical jets from accretion disks. We begin to perform a parameter space analysis by varying the amount of resistivity introduced in the disk to allow a steady accretion motion. The aim of this work is to study the effect of the resistivity in determining the properties of both accretion and ejection flows.

Key words. Accretion disks – Jets and outflows – Magnetohydrodynamics

1. Introduction

Jets and outflows are observed in very different astrophysical systems, ranging from young stars (YSO) where Herbig-Haro jets take their origin, to X-Ray binaries, up to extragalactic radio jets which are accelerated in the cores of Active Galactic Nuclei (AGN). Nowadays there is a general agreement on the fact that a similar physical scenario can explain the origin of outflows in the most diverse systems: this widely accepted model is based on the interaction of an open large-scale magnetic field with an accretion disk around a central compact object. The magnetic field extracts energy and angular momentum from the accretion disk and transfer them to the outflow which is magneto-centrifugally accelerated.

In the ideal MHD regime this mechanism has been studied for the first time by Blandford & Payne (1982) by means of self-similar steady solutions in cylindrical geometry. In that work and in the following self-similar studies that extended the model (Sakurai 1985; Contoupolos 1994; Sauty et al.; 2002) the disk is treated as a rotating boundary condition. To study the dynamics of the accretion disk and the back reaction of the jet on the disk, resistive effects must be introduced at least in the accretion disk: in fact it is necessary to allow the accretion flow to cross the poloidal magnetic field lines to obtain a steady solution (Wardle & Koenigl 1993; Casse & Ferreira 2000).

Besides of the cited analytical self-similar studies, another approach is based on numerical time-dependent simulations where, on the other hand, the problem is to deal with the large range of spatial and temporal scales involved. Most of the simulations performed were limited to the study of the outflow dynamics, treating the disk as a fixed boundary condition (Ustyugova et al. 1995; Ouyed & Pudritz 1997). Due mostly to the high computational cost, simulations which include the disk in the computational domain are performed on short time-scales (Uchida & Shibata 1985; Kato et

Send offprint requests to: C. Zanni

al. 2002) or are limited to the study of one sample case, without exploring the parameter space which defines the initial conditions (Casse & Keppens 2004; Zanni et al. 2004).

In the present work we begin to explore the parameter space by studying the effects of resistivity in determining the properties of the accretion disk and of the accelerated outflow. In Section 2 we describe the initial setup and the set of simulations that we performed, in Section 3 we analyze the acceleration and collimation mechanisms, in Section 4 we begin to study the influence of the resistivity on the asymptotic behavior of both the accretion and ejection flows, in Section 3 we analyze the outflow energetics in the different simulations while in Section 6 we give a brief summary of our results.

2. Numerical setup and simulations

To study the mechanisms which can lead to the launch of a jet from a magnetized accretion disk we perform a set of time-dependent MHD numerical simulations in axial symmetry. We use a modified 2.5D version of the MHD module provided with the FLASH multi-purpose hydrocode (`http://flash.uchicago.edu`). In the initial setup we model a Keplerian disk in equilibrium with the gravitational potential of a point-like central object. An equilibrium solution can be obtained assuming a polytropic relation between pressure and density in the disk ($P \propto \rho^\gamma$). The disk density $\rho_{\rm disk}$ is given by

$$\rho_{\rm disk} = \rho_{\rm d0}\left[\frac{\gamma-1}{\gamma\alpha_{\rm d}}\left(\frac{r_0}{R} - \epsilon^2\frac{r_0}{r}\right)\right]^{\frac{1}{\gamma-1}} \tag{1}$$

where $\gamma = 5/3$ is the adiabatic index of the plasma, $R = (r^2+z^2)^{1/2}$ is the spherical radius, r_0 is the normalization length and $\rho_{\rm d0}$ is the disk density evaluated at ($r = r_0$, $z = 0$). $\alpha_{\rm d} = c_{\rm d}^2/v_{\rm k}^2 = 0.01$ is the constant ratio between the squares of the disk isothermal sound speed $c_{\rm d}$ and the Keplerian speed $v_{\rm k}$ evaluated at the disk midplane. The initial rotation speed is given by $v_\phi = \epsilon(GM/r)^{1/2}$. The parameter $\epsilon^2 = 1 - \alpha_{\rm d}\gamma/(\gamma-1) \lesssim 1$ gives the deviation of the toroidal speed from the Keplerian value due to the gradient of the disk pressure which is given by $P_{\rm disk} = K\rho_{\rm disk}^\gamma$, with $K = v_{\rm k0}^2\rho_{\rm d0}^{1-\gamma}\alpha_{\rm d}$ ($v_{\rm k0}$ is the Keplerian speed evaluated at the cylindrical radius $r = r_0$). The disk is surrounded by a rarefied atmosphere in hydrostatic equilibrium. Assuming a polytropic relation between pressure and density, the atmosphere density $\rho_{\rm atmo}$ is defined as

$$\rho_{\rm atmo} = \rho_{a0}\left(\frac{\gamma-1}{\gamma\alpha_{\rm a}}\frac{r_0}{R}\right)^{\frac{1}{\gamma-1}} \tag{2}$$

where $\rho_{a0} = 10^{-4}\rho_{d0}$ is the corona density evaluated at $R = r_0$ and $\alpha_{\rm a} = c_{\rm a}^2/v_{\rm k}^2 = (\gamma-1)/\gamma = 0.4$ is the ratio between the squares of the atmosphere isothermal sound speed and the Keplerian speed evaluated at ($r = r_0$, $z = 0$). The equilibrium pressure is $P_{\rm atmo} = K\rho_{\rm atmo}^\gamma$ with $K = v_{\rm k0}^2\rho_{\rm a0}^{1-\gamma}\alpha_{\rm a}$. The surface at which $P_{\rm disk} = P_{\rm atmo}$ marks the boundary between the disk and the atmosphere solution. The initial magnetic field is a bent poloidal field whose magnetic energy at the disk midplane is proportional to the disk pressure, that is $\beta = 2P_{\rm disk}/B_z^2|_{z=0} = 3.33$. The precise topology of the initial magnetic field is shown in the first panel of Fig. 1 and 2. As pointed out in the Introduction, a certain amount of resistivity should be introduced in the disk to avoid the accumulation of magnetic flux and allow a steady accretion motion. In our simulations the resistivity $\nu_{\rm m}$ is parametrized following the Shakura & Sunyaev (1973) prescription for the turbulent viscosity:

$$\nu_{\rm m} = \alpha_{\rm m} V_{\rm A} H exp\left[-(z/H)^4\right] \tag{3}$$

where $V_{\rm A} = B/\sqrt{\rho}$ is the Alfven speed and $H = \sqrt{\alpha_{\rm d}}r = 0.1r$ is the height scale of the disk. The exponential function cancels the resistive effects outside the disk. $\alpha_{\rm m}$ defines the amount of resistivity which we introduce. In the present work we study the effects of resistivity by performing three simulations varying the value of $\alpha_{\rm m} = 0.1,\ 0.5,\ 1$. The computational domain of the simulations has a size $r_{\rm d} \times z_{\rm d} = 20r_0 \times 60r_0$. The equivalent resolution of the Adaptive Mesh is 256×768 points. Suitable symmetry conditions are imposed on the axis of symmetry ($r = 0$) and on the disk

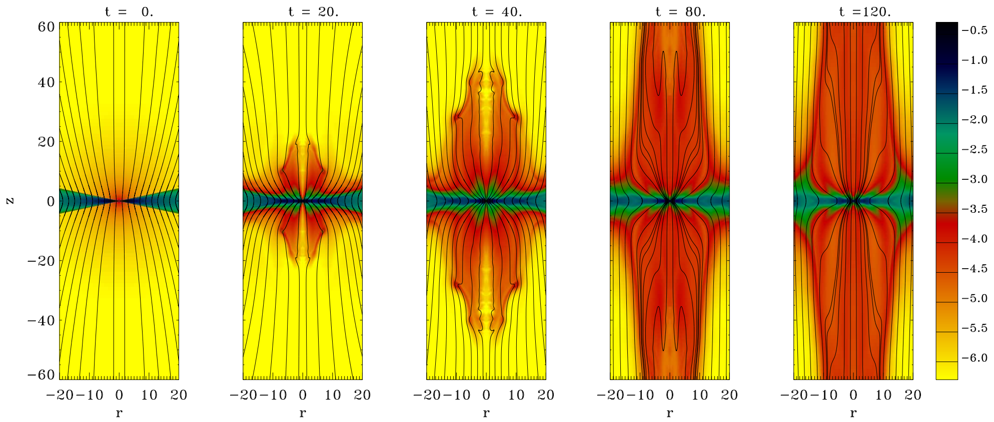

Fig. 1. Time evolution of density maps of the simulation characterized by $\alpha_m = 1$. Density is plotted in logarithmic scale and normalized on ρ_{d0}. Sample magnetic field lines are overplotted.

midplane ($z = 0$) while outflow conditions are imposed on the outer boundaries. To avoid the singularity at the origin a sink condition is imposed inside the $R < 0.5r_0$ region. In the following lengths will be given in in units of r_0, speeds in units of v_{k0} and the densities in units of ρ_{d0}. Expressed in these units the period of rotation of the disk at $r = r_0$ is equal to 2π.

3. Acceleration and collimation of the outflow

In Fig. 1 and 2 we show the time evolution of density maps of the cases characterized by $\alpha_m = 1$ and $\alpha_m = 0.1$ respectively. Following the simulation up to a time $t = 120$, which corresponds approximatively to 20 turns of the inner radius of the disk r_0, a strong outflow is produced in both simulations, although with different characteristics. First of all we can notice that due to the lower resistivity of the $\alpha_m = 0.1$ case, more magnetic flux is accumulated toward the center, causing the outflow to be hollow and unsteady. Nevertheless the mechanism which starts the launching of the jet is the same. A detailed balance of the forces which drive the dynamics of the system in the $\alpha_m = 1$ case is shown in Fig. 3: in the first panel on the left we plot cuts of the intervening forces along the z axis; we see that only the thermal pressure gradient can counteract the pinch due to both the gravitational acceleration and Lorentz force. Nevertheless the Lorentz force changes sign at the disk surface ($z \simeq 1.5$) thus driving the acceleration of the outflow. Analogously, also the toroidal component of the Lorentz force changes sign (second panel in Fig. 3): therefore the magnetic field brakes the disk, which is then losing angular momentum and accretes, while it centrifugally accelerates the outflow. The collimation of the outflow against the centrifugal pull is ensured by the radial Lorentz force (right panel in Fig. 3) which is mainly given by the tension of the toroidal field $-B_\phi^2/r$ (magnetic "hoop stress"). Even if this discussion refers specifically to the $\alpha_m = 1$ case, it is quite general and is valid for the lower resistivity cases too. The main difference in the $\alpha_m = 0.1$ case is that, due to the low resistivity, the field lines at the surface of the disk are much more bent: the greater radial component of the field generates an accelerating force in the outflow which is perpendicular to the field lines which are then continuously distorted and inverted (right panels in Fig. 2).

4. Steady accretion and ejection

Since the timescales which we are able to simulate are much shorter than the lifetime of the

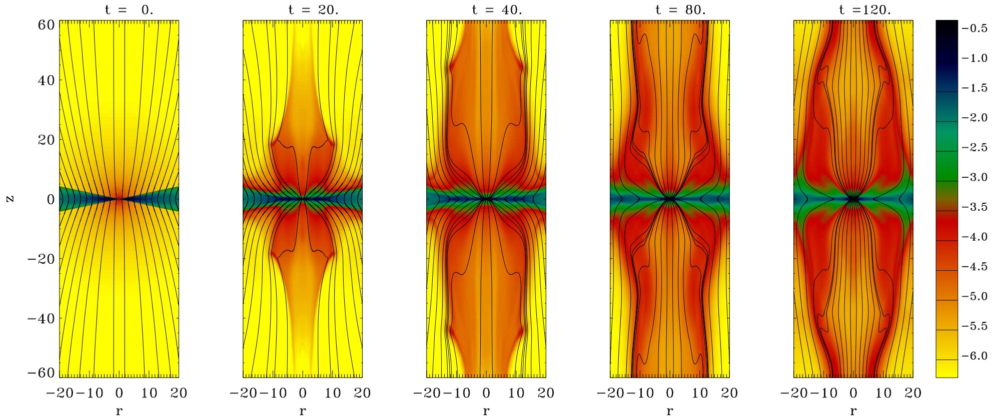

Fig. 2. Same plot as Fig. 1 for the $\alpha_\mathrm{m} = 0.1$ simulation.

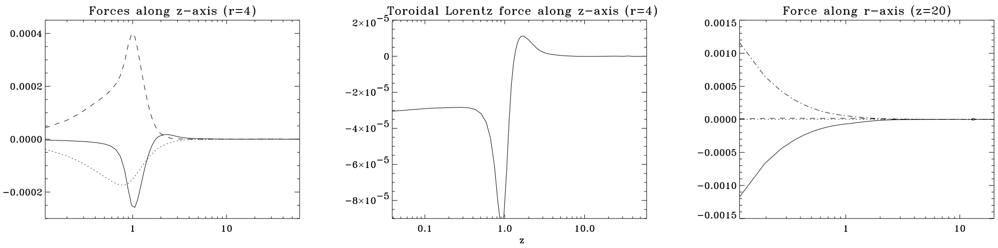

Fig. 3. Plots of the forces driving the dynamics of the $\alpha_\mathrm{m} = 1$ simulation. *Left panel*. Cuts of the forces directed along the z direction at $r = 4$: Lorentz force (*solid line*), thermal pressure gradient (*dashed line*) and gravitational acceleration (*dotted line*). *Central panel*. Cut along the z axis of the toroidal Lorentz force. *Right panel*. Cuts of the radial forces at $z = 20$: Lorentz force (*solid line*), centrifugal force (*dot-dashed line*), pressure gradient (*dashed line*) and gravitational acceleration (*dotted line*).

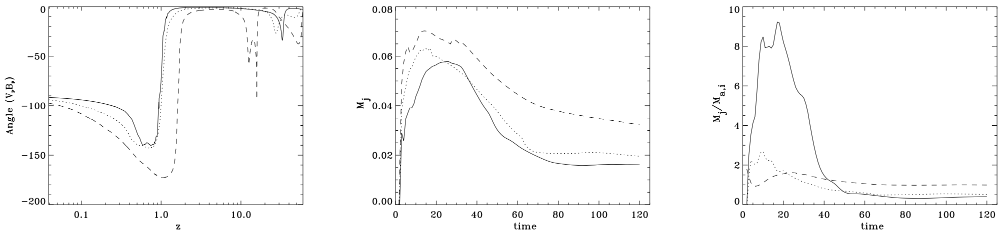

Fig. 4. *Left panel*. Angle between the poloidal speed and the poloidal magnetic field along a selected magnetic field line at $t = 120$. *Central panel*. Time evolution of the mass ejection rate calculated a the disk surface between $r = r_0$ and $r = 10r_0$. *Right panel*. Time evolution of the ratio between the ejection rate and the accretion rate on the central object. In the three panels solid lines refer to the $\alpha_\mathrm{m} = 1$ simulation, dotted lines to the $\alpha_\mathrm{m} = 0.5$ case while the dashed lines to the $\alpha_\mathrm{m} = 0.1$ simulation.

sources that we intend to model, it is important to understand if our simulations are evolving toward a steady state which can be sustained on longer timescales. In a steady state solution in the idel MHD regime the poloidal velocity should be parallel to the poloidal magnetic field lines. In the first panel on the left of Fig. 4 we plot the angle between the poloidal speed and the poloidal magnetic field along a selected magnetic field line at $t = 120$: we see that, while in the resistive disk the two vectors are almost perpendicular due to the accretion motion, in the outflow, in which the resistivity is negligible, the two vectors tend to be parallel. To evaluate the steadiness of our solutions we also plot in the second panel the mass ejection rate measured at the disk surface between $r = r_0$ and $r = 10r_0$ as a function of time: we can see that in all the three simulations, after a sudden increase, the ejection rate tends to assume an asymptotic value. We can also see that the higher is the resistivity, the lower is the rate: the lower resistivity cases develop stronger gradients of the magnetic field at the disk surface; moreover they have more opened field lines at the disk surface, thus reducing the centrifugal-gravitational potential barrier which must be overtaken to accelerate the outflow (Ogilvie & Livio 1998). In the third panel we finally plot the ratio between the mass ejection rate and the inner accretion rate on the central objects as a function of time: we obtain asymptotic ratios around $\simeq 1,\ 0.5$ and 0.4 for $\alpha_{\rm m} = 0.1,\ 0.5,\ 1$ respectively. A ratio equal to 1 means that an equal amount of mass coming from the outer accretion goes into the outflow and onto the central object.

5. Energy balance of the outflow

We finally study which are the main differences in the energetics of the outflows produced by disks characterized by a different resistivity. In the first panel in Fig. 5 we plot the energy flux integrated at the disk surface between $r = r_0$ and $r = 10r_0$ as a function of time; the energy flux is given by the sum of the Poynting flux $(\mathbf{v} \times \mathbf{B}) \times \mathbf{B}$ and the kinetic flux $= 1/2\rho v^2\mathbf{v}$. We see that asymptotically the outflows generated in the three simulations are extracting about the same amount of energy from the disk. Differences can be found when we plot the ratio between the Poynting flux and the kinetic flux as a function of the z coordinate along the outflow (second panel of Fig. 5): outflows with a lower ejection rate, which are then produced by a disk with a higher resistivity, show a higher ratio between the two fluxes at the disk surface. On the disk scale the Poynting flux mainly determines the extraction of specific angular momentum from the disk (see Zanni et al. 2004): our results show then that the lower is the mass loading of the outflow, the more efficient is the magneto-centrifugal process which accelerates the outflow. Since the Poynting flux which is dominant on the disk height scale is then transferred to the kinetic flux along the outflow (second panel in Fig. 5), the asymptotic speed of the outflow is therefore higher for jets with a lower mass flux (third panel in Fig. 5). The asympototic speeds are around the escape velocity and super-fastmagnetosonic.

6. Summary

The simulations presented in this paper allowed us to study in detail the mechanisms which are responsible for the acceleration and collimation of astrophysical jets. Our results showed how a poloidal magnetic field threading a Keplerian disk can extract angular momentum from the disk itself and transfer it to an outflow which is therefore centrifugally accelerated. Moreover the extraction of angular momentum allows the disk to accrete on the central object. We performed a series of three simulations varying the resistivity of the disk characterized by the adimensional parameter $\alpha_{\rm m} = 0.1,\ 0.5,\ 1$. We therefore studied how the accretion and ejection processes are affected by a different resistivity showing that less resistive disks produce higher ejection rates. Due to the different ejection rates also the outflow showed different properties: the magneto-centrifugal mechanism driving the acceleration is more efficient in the jets with a lower mass ejection rate thus producing a higher terminal speed. Nevertheless the total energy flux extracted by the outflow through the disk surface

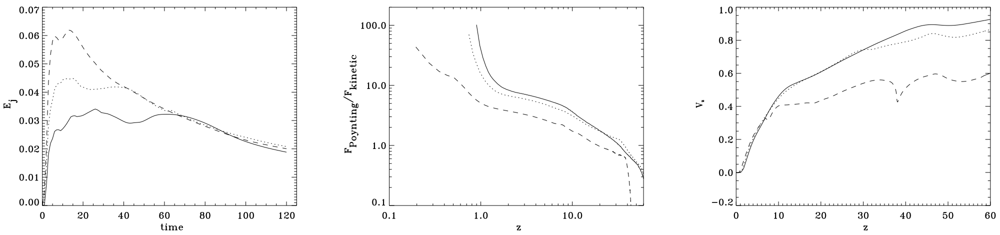

Fig. 5. *Left panel*. Time evolution of the energy flux through the disk surface between $r = r_0$ and $r = 10r_0$. The flux is given by the sum of the kinetic and the Poynting flux. *Central panel*. Plot of the average ratio between Poynting and kinetic fluxes along the outflow at the final simulated time $t = 120$. *Right panel*. Plot of the average z component of the jet speed along the outflow at $t = 120$. In the three panels solid lines refer to the $\alpha_m = 1$ simulation, dotted lines to the $\alpha_m = 0.5$ case while the dashed lines to the $\alpha_m = 0.1$ simulation.

was similar at the final simulated time for all the three cases studied.

Acknowledgements. The software used in this work was in part developed by the DOE–supported ASCI/Alliance Center for Astrophysical Thermonuclear Flashes at the University of Chicago. This work has been co–funded by MIUR under the grant 2002028843. The numerical calculations have been performed at CINECA in Bologna, Italy, thanks to the support of INAF.

References

Blandford, R. D., & Payne, D. G. 1982, MNRAS, 199, 883
Casse, F. & Ferreira, J. 2000, A&A, 353, 1115
Casse, F. & Keppens, R. 2004, ApJ, 601, 90
Contopoulos, J. 1994, ApJ, 432, 508
Kato, S., Kudoh, T. & Shibata, K. 2002, ApJ, 565, 1053
Ogilvie, G. I. & Livio, M. 1998, ApJ, 499, 329
Ouyed, R. & Pudritz, R. 1997, ApJ, 482, 712
Sakurai, T. 1985, A&A, 39, 821
Sauty, C., Trussoni, E. & Tsinganos, K. 2002, A&A, 389, 1068
Shakura, N. I. & Sunyaev, R. A., 1973, A&A 24, 337
Uchida, Y., & Shibata, K. 1985, PASJ, 37, 515
Ustyugova, G. V., Koldoba, A. V., Romanova, M. N., Chetchetkin, V. M. & Lovelace, R. V. E. 1995, ApJ, 439, L39
Wardle, M. & Koenigl, A. 1993, ApJ, 410, 218
Zanni, C., Ferrari, A., Massaglia, S., Bodo, G., & Rossi, P. 2004 Ap&SS, 293, 99